

May 31, 2022

Single-electron transport in InAs nanowire quantum dots formed by crystal phase engineering

Malin Nilsson¹, Luna Namazi¹, Sebastian Lehmann¹, Martin Leijnse¹, Kimberly A. Dick^{1,2}, and Claes Thelander¹¹*Division of Solid State Physics and NanoLund,
Lund University, Box 118, S-221 00 Lund, Sweden and*²*Center for Analysis and Synthesis, Lund University, Box 124, S-221 00 Lund, Sweden*

We report electrical characterization of quantum dots (QDs) formed by introducing pairs of thin wurtzite (WZ) segments in zinc blende (ZB) InAs nanowires. Regular Coulomb oscillations are observed over a wide gate voltage span, indicating that WZ segments create significant barriers for electron transport. We find a direct correlation of transport properties with quantum dot length and corresponding growth time of the enclosed ZB segment. The correlation is made possible by using a novel method to extract lengths of nanowire crystal phase segments directly from scanning electron microscopy (SEM) images, and with support from transmission scanning microscope (TEM) images of typical nanowires. From experiments on controlled filling of nearly empty dots with electrons, up to the point where Coulomb oscillations can no longer be resolved, we estimate the ZB/WZ conduction band offset to approximately 95 meV.

PACS numbers: 73.23.Hk 73.63.Kv 73.63.Nm 61.05.-a

Keywords: Quantum dot, single electron tunneling, crystal phase engineering, zinc blende, wurtzite, polytypism, InAs, MOVPE

I. INTRODUCTION

Epitaxially-grown semiconductor nanowires often have an uncontrolled mix of crystal phases, most commonly wurtzite (WZ) and zinc blende (ZB). Considerable efforts have been made to find growth conditions where a single, defect-free crystal phase is formed, which is required in many applications in electronics and optics. Of special interest is the WZ phase, which is unique to nanowires for the non-nitride III-V semiconductors. At the same time, new methods for crystal-phase control in nanowires have been used to controllably switch crystal phase in the growth direction of a single nanowire, creating a so-called homostructure.¹ Importantly, such crystal phase junctions can be tuned to be atomically abrupt, and can be formed e.g. by metal-organic vapor phase epitaxy (MOVPE).

Homostructures consisting of thin segments of ZB and WZ have been optically studied in InP and GaAs nanowires,^{2,3} resulting in a further understanding of effects of polytypism on the band structure in those material systems. In the case of InAs, a material with strong relevance for future low-power electronics, it has been theoretically predicted that WZ has a larger bandgap than ZB,⁴ with a positive conduction band off-set of up to 126 meV.^{5,6} Mixing of the crystal phases in a nanowire device is therefore expected to strongly affect the electrical properties.^{7,8}

Efforts have been made to study the band alignment at the interface between ZB and WZ in InAs nanowires, yet few experimental results have been reported to support the theoretical predictions, partly explained by the difficulties involved in optical studies due to the narrow band gap ($E_g = 0.354$ eV in ZB at 295 K). Another com-

plication is that the polar $\{0001\}/\{000\bar{1}\}$ -type surfaces of WZ are expected to have polarization charges at the interfaces to the ZB, which should modify the band structure at the junction.^{9,10} However, for InAs, the amount of polarization charge relative to surface charges is unknown. Recent results from surface analysis of hydrogen-cleaned InAs nanowires show no detectable polarization charges at the interface or off-set in the conduction band; the latter was explained by the intrinsic n-type characteristic of InAs masking the fundamental off-set.¹¹ In addition, the authors in Ref. 11 point out the importance of surface states and surface oxides on the band alignment. In experiments on InAs nanowires *with* native oxides, thermionic emission measurements indicate that WZ forms barriers relative to ZB for electron transport.⁸ The latter is also supported by the observation that very thin WZ segments in an otherwise ZB InAs nanowire act as tunnel barriers for electrons; pairs of such WZ barriers enclosing a ZB segment, show single-electron charging at low temperatures, thus forming a quantum dot (QD).¹²

The electronic properties of InAs WZ-ZB junctions have become even more relevant by recent demonstrations that radial heterostructures can be formed selectively on ZB segments, whereas radial growth is effectively suppressed on WZ.^{13–15} Nanowire core-templates consisting of InAs double-barrier WZ structures could thus be used to realize enclosed ZB quantum dots with an InAs-GaSb core-shell geometry, which would be of considerable interest for studies of electron-hole interactions.¹⁶

In this work, we present results on InAs nanowire homostructure QDs using a growth method that, compared to Ref. 12, involves higher growth temperature and an improved method to induce structural changes by change

of group V/III precursor flow ratio.^{15,17} The new conditions allow a reduction in both impurity incorporation and QD-size, which facilitates observation of Coulomb blockade and various quantum confinement-related effects at 4.2 K. By correlating the length of ZB QDs with the frequency of Coulomb oscillations induced by the gate, we can confirm the role of the WZ segments as tunnel barriers. Coulomb blockade is observed over a wide range of gate voltages which, converted to an energy scale, provides a lower estimate of the conduction band offset between WZ and ZB of around +95 meV.

Furthermore, as transmission electron microscopy (TEM) characterization is extremely difficult to carry out on nanowires on which 3-terminal electrical measurements are performed, we have developed a new approach to accurately extract lengths and volumes of nanowire crystal phase segments using electron channeling contrast imaging (ECCI) in scanning electron microscopy (SEM).¹⁸

II. METHOD

InAs nanowires containing crystal-phase defined QDs were grown by means of metal organic vapor phase epitaxy (MOVPE) on $(\bar{1}\bar{1}\bar{1})$ oriented InAs substrates with predeposited aerosol Au seed particles. The particles used for this study were 40 nm in diameter with an areal density of 1 particle per μm^2 . A low-pressure MOVPE reactor from Aixtron with a total precursor flow of 13 l/min and operated at a pressure of 100 mbar was utilized with Trimethylindium (TMIn) and Arsine (AsH_3) as precursors. Prior to growth, the samples were annealed under H_2/AsH_3 at an elevated set temperature of 550 °C to remove native oxides from the surface of the substrate. Subsequently, the growth temperature was set to 460 °C. Different V/III ratios were employed for growing the WZ and ZB crystal structures by changing the molar fraction of both growth species; AsH_3 was set to $9.23 \cdot 10^{-5}$, and $1.54 \cdot 10^{-2}$, while TMIn was set to $3.48 \cdot 10^{-6}$, and $1.93 \cdot 10^{-6}$ for the WZ and ZB segments, respectively. The lengths of the segments were scaled and controlled with the set growth time. The two segments of WZ were both grown for 5 s, whereas the enclosed ZB segment was grown for either 40 or 20 s for the two sets of nanowire samples studied in this paper. These samples will be referred to as Sample 1 and 2, respectively.

TEM analysis was carried out in a JEOL 3000F setup operated at 300 kV where the nanowires were mechanically broken-off the growth substrate before transferring them onto lacey carbon covered copper grids. A Zeiss Leo Gemini 1560 was used for acquisition of SEM data with a typical acceleration voltage of 15 kV and beam currents on the order of 100 μA . Sample tilts in the range of -5 ° to 20 ° were set to ensure satisfactory conditions for ECCI to distinguish WZ and ZB segments in the nanowires.

Nanowire devices were fabricated by mechanically transferring nanowires from the growth samples to de-

generately n-doped silicon substrates with a 110 nm thick SiO_2 film. Such a substrate has predefined gold markers and contact pads, and the back side is covered with gold. The doped Si substrate serves as a global back gate during the electrical measurements. Source- and drain contacts consisting of 250 nm Ni and 750 nm Au and were processed by electron beam lithography, followed by lift-off. A 30 s O_2 -plasma etch and an $\text{HCl}:\text{H}_2\text{O}$ (1:20) etch for 10 s were carried out prior to metallization to remove resist residue and native oxide, respectively.

III. RESULTS & DISCUSSION

A schematic representation of the nanowire structure is shown in Fig. 1(a), together with a sketch of the conduction band edge E_{CB} alignment based on the simplified assumption that WZ forms a square potential barrier relative to ZB [Fig. 1(b)]. The WZ segments (dark blue) define a small quantum dot in an otherwise ZB (light blue) nanowire, and the stripes in the ZB segments represent twinned segments, unintentionally incorporated during growth. It has previously been reported that such twinned segments do not affect the resistivity in InAs nanowires at 295 K, suggesting that other sources of scattering are limiting transport, such as surface states.⁸ As will be shown, no discernible transport phenomena that can be attributed to twinned segments are found in this study.

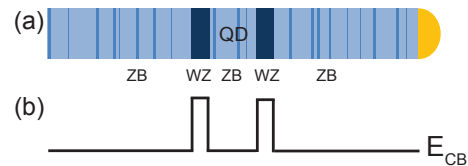


FIG. 1: (Color online) (a) Schematic of the nanowire crystal structure composition, where the QD is defined by WZ segments (dark blue) in an otherwise ZB (light blue) nanowire. The stripes in the ZB segments represent twinned segments. (b) Sketch of the conduction band edge E_{CB} of the system, where the WZ segments are represented by simple square potential barriers.

We find distinct effects of the WZ barriers on conductivity and pinch-off voltage compared to ZB reference samples. Conductivity as a function of gate voltage for a QD device (Sample 1) and over a reference ZB segment (Sample 1) at 295 K and 4.2 K are displayed in Fig. 2(a) and (b), respectively. The contact configurations in the two cases are shown in the cartoons in Fig. 2(c). A clear suppression in conductivity is visible at 295 K for the QD device compared to the reference ZB segment, and at 4.2 K we find a difference in pinch-off voltage of around 10 V. This is in contrast to what was previously reported in Ref. 12, where no dramatic effects on the current levels and pinch-off voltage for QD structures consisting of 4 nm WZ barriers separated by a 130 nm ZB segment were ob-

served. This could be explained by the much thinner WZ barriers used in that study compared to those studied in this work. Measurements on more QD and reference ZB devices at 4.2 K are displayed in Fig. 1(a) in the supplementary information (SI). Figure 1(b) in the SI shows SEM images of the reference ZB devices where twinned segments can clearly be seen. This confirms that the WZ segments are responsible for the increased resistance, and that these have a much stronger effect on conductance than twinned segments, which was indirectly shown in Ref. 8.

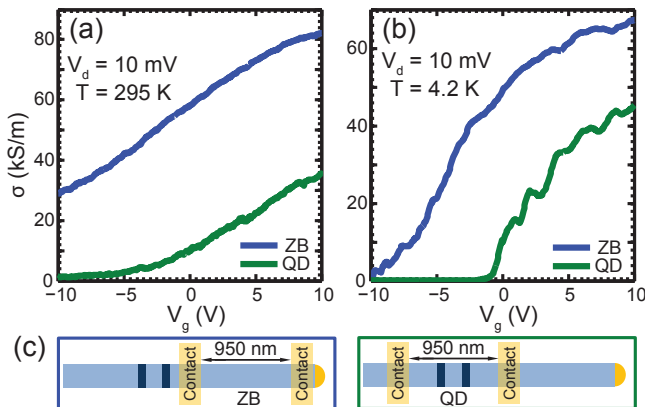


FIG. 2: (Color online) Conductivity as a function of gate voltage V_g measured over a QD structure (blue) and over a reference ZB segment (green), at (a) $T = 295$ K, (b) $T = 4.2$ K. The length and diameter of the QD are 45 nm and 78 nm, respectively, and the thicknesses of the WZ barriers are 22 nm and 19 nm. The accuracy of the dimensions extracted from SEM analysis is estimated to be ± 2 nm. (c) Schematic drawings of the contact configurations for the nanowires measured.

Next, the role of the WZ segments in low-temperature charge transport is studied. Conductance as a function of gate voltage at a bias of 0.36 mV for a typical QD device (Sample 1) at 4.2 K is displayed in Fig. 3. The graph is a composite of several sequential measurements, following Coulomb oscillations from depletion (~ -7 V), to a point where the oscillations cease (~ 0 V). Well-defined Coulomb oscillations, observable over a wide range in gate voltage, is a general behavior for the QD devices in this study, which demonstrates that the double WZ segments create significant tunnel barriers in the conduction band. Close to depletion the Coulomb peaks are somewhat irregularly spaced, which is commonly observed in few-electron QDs.¹⁹ Fourier transform analysis of the Coulomb peaks show that this initial irregularity is followed by more than a hundred peaks with nearly constant frequency. Figure 3 shows that the conductance overall increases with gate voltage; this is attributed to an increase in both tunnel probability and thermionic emission over the barriers, as well as an on-set of co-tunneling when the effective barrier height decreases.

The inset in Fig. 3 show a top-view SEM image of the measured device, a high resolution SEM image of the

QD structure together with an intensity profile. From the high resolution SEM image, the nanowire and QD-dimensions can be extracted using ECCI. The latter indicates a 75 nm diameter nanowire, with a pair of 20 nm WZ segments enclosing a 53 nm ZB segment. Here we have used a new approach that exploits ECCI to deduce the crystal phase directly from SEM images, enabled by careful correlation with information from nanowires studied by TEM only, which we will now discuss in more detail.

Figures 4(a) and (b) display high resolution TEM images of nanowires from Sample 1 (longer QD) and 2 (shorter QD), respectively. Blue (ZB) and red (WZ) shadings are used to indicate the crystal phase of the nanowire; the darker blue indicates the QD. In the close up in panel (a), the atomically sharp transition between the crystal phases is clearly visible. Nanowires from both samples exhibit a ZB phase with rotational twinning perpendicular to the $[\bar{1}\bar{1}\bar{1}]$ growth axis of the nanowire, which can be seen as bright and dark contrast areas in the TEM images.

Figure 4(c) shows an SEM image of a QD device (Sample 1). Aligning the electron beam with the crystal planes in the nanowire allows the crystal phases to be distinguished with ECCI, and the QD-dimensions to be extracted, thus making it possible to directly correlate electrical properties with structural properties. Depending on the alignment of the nanowire with respect to the electron beam, the contrast between WZ and ZB can vary. Furthermore, the conditions at which twinned ZB segments can be distinguished do not necessarily overlap with conditions where it is possible to distinguish between ZB and WZ, for more details see the SI. From the SEM analysis we find that the nanowire in Fig. 4(c) has 35 nm thick WZ segments enclosing an 81 nm long ZB segment. For all dimensions extracted from SEM analysis in this work, we estimate an accuracy of ± 2 nm.

The use of randomly distributed aerosol seed particles in the growth results in a substantial spread in the QD-dimensions. However, this spread is not a limitation in this study since the dimensions can be extracted from SEM analysis after the electrical measurements. There are two major factors that affect the QD-dimensions and segment lengths: First, there is a direct correlation between seed particle size and nanowire diameter, such that a spread in gold particle diameter will give a corresponding spread in nanowire growth rate and quantum dot dimensions.²⁰ Second, nanowire growth rate is also affected by local variations in particle density on the growth substrate.^{20,21}

Next, the electrical properties of several QDs at $T = 4.2$ K are correlated to the QD-dimensions extracted from SEM images. Figures 5(a) - (d) show measurements of conductance as a function of gate voltage recorded for four QD devices with different dimensions, as well as cartoons of the corresponding QD structures. (a) - (c) represent nanowires grown with a longer growth time (40 s) for the ZB QD segment, whereas (d) represent a

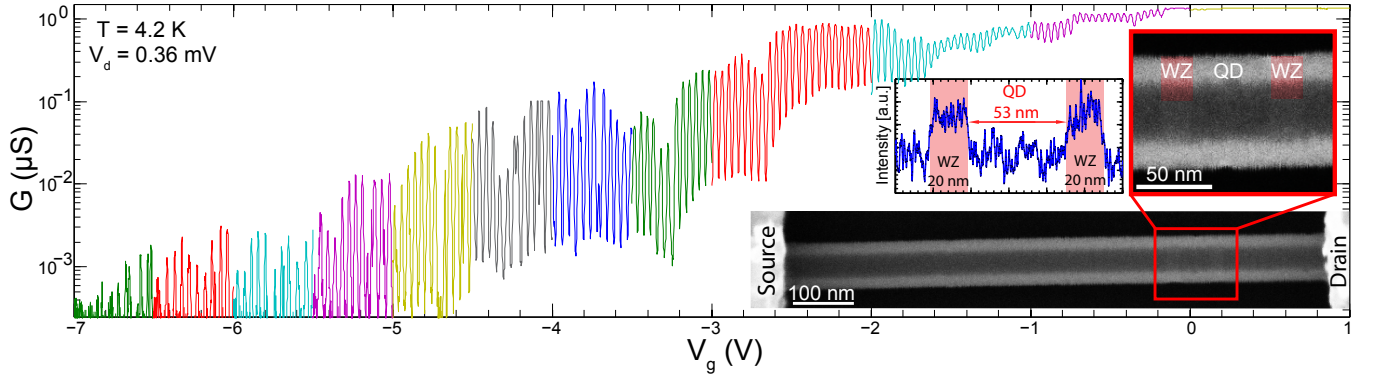


FIG. 3: (Color online) Composite of sequential conductance measurements as a function of gate voltage, discriminated by color. Inset: (Bottom) top view SEM image of the corresponding device, (top right) a high resolution SEM of the QD structure where parts of the WZ segments has been colored red to guide the eye, and (top left) corresponding intensity profile where the lengths of the QD and barriers are indicated.

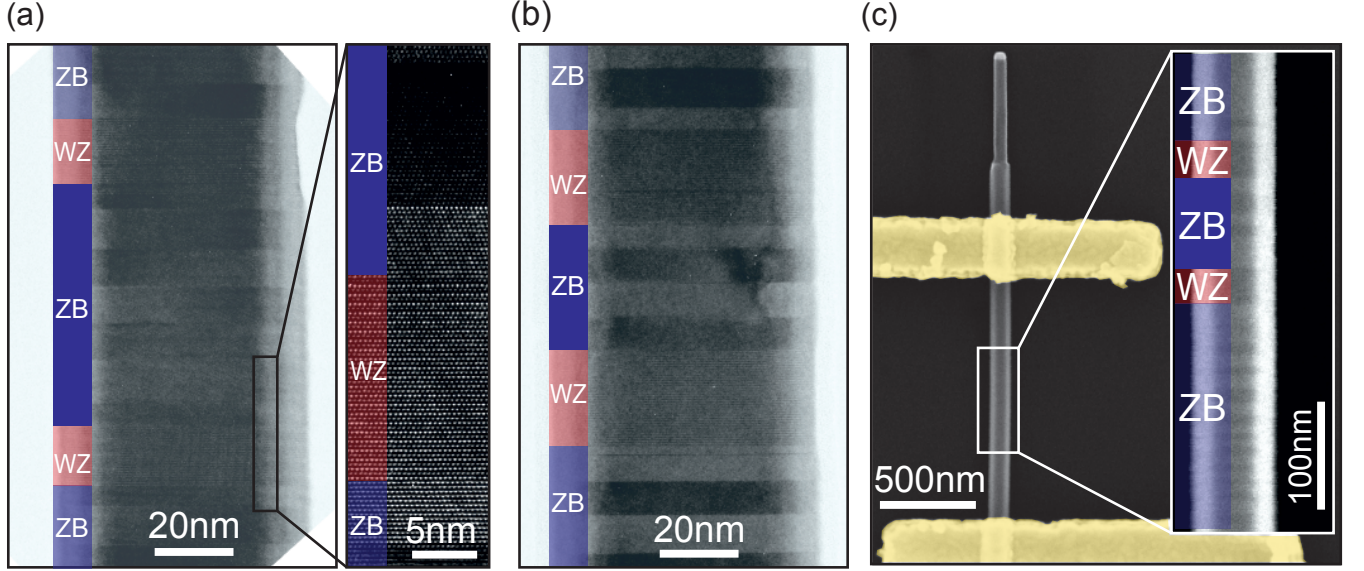


FIG. 4: (Color online) (a) and (b) TEM images of nanowires from Samples 1 and 2, respectively. In the close up in (a) the crystal phase can be distinguished. Dimensions extracted from (a): WZ barrier lengths 16 nm/20 nm, ZB QD length 60 nm and diameter of ZB QD 64 nm. Dimensions extracted from (b): WZ barriers lengths 25 nm/25 nm, ZB QD length 32 nm and diameter of ZB QD 69 nm. The accuracy of the dimensions is ± 1 nm. (c) SEM image of a nanowire device. (Sample 1), from the close up crystal phase transitions and twinned ZB segments can be mapped out. For electrical measurements see Fig. 5(a) and (e).

nanowire grown with a shorter growth time (20 s) for the QD segment. Figures 5(e) and (f) show charge stability diagrams recorded for the same devices as displayed in (b) and (d), respectively.

Regular Coulomb oscillations are clearly visible for all QD devices in Fig. 5(a) - (d), where the oscillations continue over gate voltage ranges of 5-7 V, showing that the WZ segments introduce a significant conduction band offset. As expected for QD-systems in the quantum Coulomb blockade regime ($kT \ll$ single particle energy E_Δ , and charging energy E_C), the amplitude of the Coulomb peaks is gate-voltage dependent. This

dependence is due to different tunnel coupling strengths between conducting modes in the leads and states on the dot, in combination with an energy-dependent density of states in the leads.

In the case of the three QDs in Fig. 5(a) - (c), the Coulomb oscillation frequency is nearly constant, indicating that E_C is much larger than E_Δ , and is the dominating term in the addition energy ($E_{Add} = E_C + E_\Delta$). In (e), this is evident from the equal size of the Coulomb diamonds. From charge stability diagrams, charging energies ($E_C = e\Delta V_d$) of 4.3 meV, 4.0 meV, and 4.5 meV and nearly constant gate capacitances ($C_g = \frac{e}{\Delta V_g}$) of

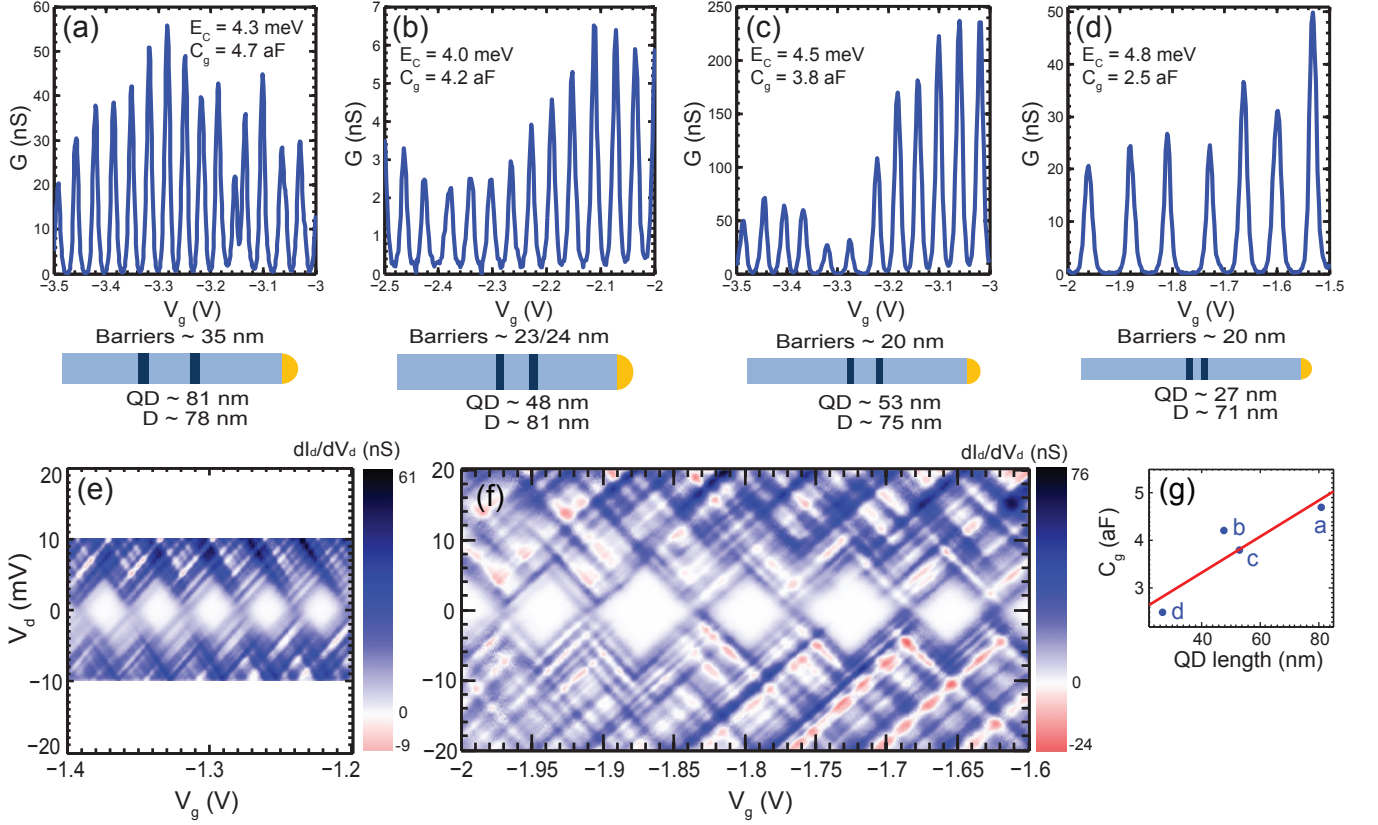


FIG. 5: ((Color online) (a) - (d) Coulomb oscillations in conductance as a function of gate voltage for quantum dots with different lengths, (a) 81 nm, (b) 48 nm, (c) 53 nm (same device as in Fig. 3) and (d) 27 nm, and cartoons (not to scale) of corresponding QD structures. In the cartoons, *Barriers* denotes the width of the WZ segments (dark blue), *QD* denotes the QD length and *D* denotes the nanowire diameter. All measurements were performed at $T = 4.2$ K with a bias of $V_d = 0.36$ mV. (e) and (f) Charge stability diagrams of same devices as (b) and (d), respectively, at $T = 4.2$ K. Positive conductance lines running perpendicular to the diamond edges are visible in both stability diagrams, and correspond to the on-set of sequential tunnel transport via excited states. In addition to these lines, negative conductance lines running parallel to the excited states are visible, which we attribute to fluctuations in tunnel probability between conducting modes in the leads and states in the QD as mentioned in the text. (g) Extracted gate capacitance vs. length of the QD for the four devices, respectively. The red line is a linear fit to the data points.

approximately 4.8 aF, 4.2 aF, and 3.8 aF are extracted for the three devices, respectively. Here, ΔV_d and ΔV_g are the maximum height (measured from $V_d = 0$) and the total width (measured at $V_d = 0$) of the Coulomb blockade diamond, respectively.

When the length of the QD is reduced to 27 nm, the contribution of E_Δ can be resolved as irregular Coulomb peak spacings with an odd-even behavior [Fig. 5(d)], which is also clearly visible in the charge stability diagram [Fig. 5(f)]. In this case, a charging energy of approximately 4.8 meV, and a reduced gate capacitance of 2.5 aF, as well as a constant E_Δ of 1.4 meV, are extracted. In the case of a stability diagram recorded at more negative gate voltages (-3 to -2.6 V), the extracted E_Δ increases to 2 - 4 meV.

In order to correlate the dimensions of the QD devices with their electrical properties, the gate capacitance vs. length of the QDs is shown in Fig. 5(g), together with a linear fit to the data points (red line). The trend shows a

scaling of C_g with the length of the QD segment, clearly indicating that the WZ segments act as tunnel barriers, and effectively define a QD.

Next we extract a lower limit for the WZ conduction barrier offset relative to ZB by estimating the electron population and concentration on the quantum dot at the point where the Coulomb oscillations cease. At that point the Fermi level is assumed to be aligned with the top of the WZ barriers, and thus the position of the Fermi level E_F relative to the ZB conduction band edge E_{CB} provides an estimate of the conduction band offset. The electron density n on a dot is calculated from the number of observed Coulomb oscillations divided by the QD-volume extracted from an SEM image. By evaluating the following expression for the electron density, where the nonparabolicity of the band is compensated for, $(E_F - E_{CB})$ can be extracted:^{22,23}

TABLE I: Extracted dimensions, number of electrons and, electron concentration n in the QD at the point where Coulomb oscillations cease, and calculated barrier heights ($E_F - E_{CB}$) for three QD devices. All three devices consisted of nanowires from growth Sample 1.

Device	Diameter (nm)	QD length (nm)	WZ barrier lengths (nm)	# of electrons	n (cm^{-3})	Barrier height (meV)
A	83	61	33/37	217	$6.6 \cdot 10^{17}$	95
B [Fig. 3, Fig. 4(c)]	75	53	20	159	$6.8 \cdot 10^{17}$	97
C [Fig. 2]	78	45	22/19	139	$6.5 \cdot 10^{17}$	94

$$n = \frac{2N_C}{\sqrt{\pi}} \int_0^\infty \frac{\sqrt{\varepsilon(1+\alpha\varepsilon)}(1+2\alpha\varepsilon)}{1+\exp(\varepsilon-\phi)} d\varepsilon. \quad (1)$$

Here, N_C is the effective density of states in the conduction band, $\varepsilon = (E - E_{CB})/kT$ is the normalized electron kinetic energy, $\phi = (E_F - E_{CB})/kT$ is the normalized Fermi energy and $\alpha = (1 - \frac{m_e}{m_0})^2/\varepsilon_g$ is the non-parabolicity factor, containing the effective mass m_e and the normalized band gap $\varepsilon_g = E_g/kT$. The system is assumed to be in the extreme degeneracy/low temperature regime $E_F - E_{CB} \gg kT = 0.36$ meV) where a step-function approximation of the Fermi function in the evaluation of Eq. (1) can be used. In this estimation, we have assumed that the effect of the gate on the conduction band edge is constant in all ZB segments, and quantum confinement has been neglected.

Three devices have been analyzed, which resulted in barrier heights of 95 meV, 97 meV, and 94 meV, respectively; details of the devices are stated in Table I. For InAs {110}-type surfaces with a thin oxide, the Fermi level is reported to be pinned approximately 100 meV above the conduction band edge.^{24,25} This is consistent with the Fermi level position at $V_g = 0$ V found here, which coincidentally also is the point at which the Coulomb blockade due to the WZ segments is lifted in most samples studied.

IV. SUMMARY

In summary, we demonstrate controlled formation of QDs in nanowires through polytypic design. The QDs are

formed by introducing pairs of thin, closely spaced segments of WZ, in otherwise ZB InAs nanowires. Coulomb oscillations with reproducible periodicity are observed over a wide gate voltage span, indicating a significant conduction band offset. A novel method is developed to extract QD-dimensions and barrier widths directly from SEM images, which is used in the analysis of the electrical measurement data. With this information, it is possible to directly correlate electrical properties of the QDs, such as gate capacitance and charging energy, with the dimensions of the crystal phase segments. Confinement effects can be clearly resolved for the shortest QD lengths where $kT \ll E_\Delta$ at 4.2 K. Based on estimations of the carrier concentrations in longer QDs by counting Coulomb oscillations, we extract a ZB-WZ conduction band offset of approximately 95 meV. In view of recent findings that WZ nanowire surfaces can effectively inhibit radial overgrowth,¹⁵ we finally conclude that polytype control may offer a path to realize more complex systems, such as epitaxially designed core-shell QDs.

Acknowledgments

This work was carried out with financial support from NanoLund, the Swedish Research Council (VR), the Swedish Foundation for Strategic Research (SSF), and the Knut and Alice Wallenberg Foundation (KAW).

- ¹ P. Caroff, K. A. Dick, J. Johansson, M. E. Messing, K. Deppert, and L. Samuelson, *Nature Nanotechnology* **4**, 50 (2009).
- ² N. Akopian, G. Patriarche, L. Liu, J.-C. Harmand, and V. Zwiller, *Nano Lett.* **10**, 1198 (2010).
- ³ N. Vainorius, S. Lehmann, D. Jacobsson, L. Samuelson, K. A. Dick, and M.-E. Pistol, *Nano Lett.* **15**, 2652 (2015).
- ⁴ Z. Zanolli, F. Fuchs, J. Furthmüller, U. von Barth, and F. Bechstedt, *Phys. Rev. B* **75**, 245121 (2007).

- ⁵ M. Murayama and T. Nakayama, *Phys. Rev. B* **49**, 4710 (1994).
- ⁶ A. Belabbes, C. Panse, J. Furthmüller, and F. Bechstedt, *Phys. Rev. B* **86**, 075208 (2012).
- ⁷ M. D. Schroer and J. R. Petta, *Nano Lett.* **10**, 1618 (2010).
- ⁸ C. Thelander, P. Caroff, S. Plissard, A. W. Dey, and K. A. Dick, *Nano Lett.* **11**, 2424 (2011).
- ⁹ S. A. Dayeh, D. Susac, K. L. Kavanagh, E. T. Yu, and D. Wang, *Advanced Functional Materials* **19**, 2102 (2009).

- ¹⁰ A. Belabbes, J. Furthmüller, and F. Bechstedt, *Phys. Rev. B* **87**, 035305 (2013).
- ¹¹ M. Hjort, S. Lehmann, J. Knutsson, A. A. Zakharov, Y. A. Du, S. Sakong, R. Timm, G. Nylund, E. Lundgren, P. Kratzer, et al., *ACS Nano* **8**, 12346 (2014).
- ¹² K. A. Dick, C. Thelander, L. Samuelson, and P. Caroff, *Nano Lett.* **10**, 3494 (2010).
- ¹³ K. Kawaguchi, M. Heurlin, D. Lindgren, M. T. Borgström, M. Ek, and L. Samuelson, *Appl. Phys. Lett.* **99**, 131915 (2011).
- ¹⁴ T. Rieger, M. Luysberg, T. Schäpers, D. Grützmacher, and M. I. Lepsa, *Nano Lett.* **12**, 5559 (2012).
- ¹⁵ L. Namazi, M. Nilsson, S. Lehmann, C. Thelander, and K. A. Dick, *Nanoscale* **7**, 10472 (2015).
- ¹⁶ B. Ganjipour, M. Leijnse, L. Samuelson, H. Q. Xu, and C. Thelander, *Phys. Rev. B* **91**, 161301 (2015).
- ¹⁷ S. Lehmann, J. Wallentin, D. Jacobsson, K. Deppert, and K. A. Dick, *Nano Lett.* **13**, 4099 (2013).
- ¹⁸ D. C. Joy, D. E. Newbury, and D. L. Davidson, *J. Appl. Phys.* **53**, R81 (1982).
- ¹⁹ L. P. Kouwenhoven, C. M. Marcus, P. L. Mceuen, S. Tarucha, M. W. Robert, and N. S. Wingreen, *Kluwer Series* **E345** (1997).
- ²⁰ L. E. Fröberg, W. Seifert, and J. Johansson, *Phys. Rev. B* **76**, 153401 (2007).
- ²¹ M. T. Borgström, G. Immink, B. Ketelaars, R. Algra, and E. P. Bakkers, *Nature Nanotechnology* **2**, 541 (2007).
- ²² V. Ariel-Altschul, E. Finkman, and G. Bahir, *IEEE Transactions on Electron Devices* **39**, 1312 (1992).
- ²³ E. Lind, Y.-M. Niquet, H. Mera, and L.-E. Wernersson, *Appl. Phys. Lett.* **96**, 233507 (2010).
- ²⁴ H. U. Baier, L. Koenders, and W. Mönch, *Solide State Commun.* **58**, 327 (1986).
- ²⁵ D. C. Tsui, *Phys. Rev. Lett.* **24**, 303 (1970).

Supplementary Information

Single-electron transport in InAs nanowire quantum dots formed by crystal phase engineering

Malin Nilsson¹, Luna Namazi¹, Sebastian Lehmann¹, Martin Leijnse¹, Kimberly A. Dick^{1,2}, and Claes Thelander¹

¹*Division of Solid State Physics and NanoLund,
Lund University, Box 118, S-221 00 Lund, Sweden and*

²*Center for Analysis and Synthesis, Lund University, Box 124, S-221 00 Lund, Sweden*

For statistics on the impact of the QD structure on the conductivity, see Fig. 1(a), where conductivity is plotted as a function of gate voltage for four reference ZB devices and four QD devices. Figure 1(b) shows SEM images of the reference ZB devices with visible contrast originating from twinned segments, strongly indicating the weak impact of the twinned segments on the current level compared to the WZ segments in the QD devices.

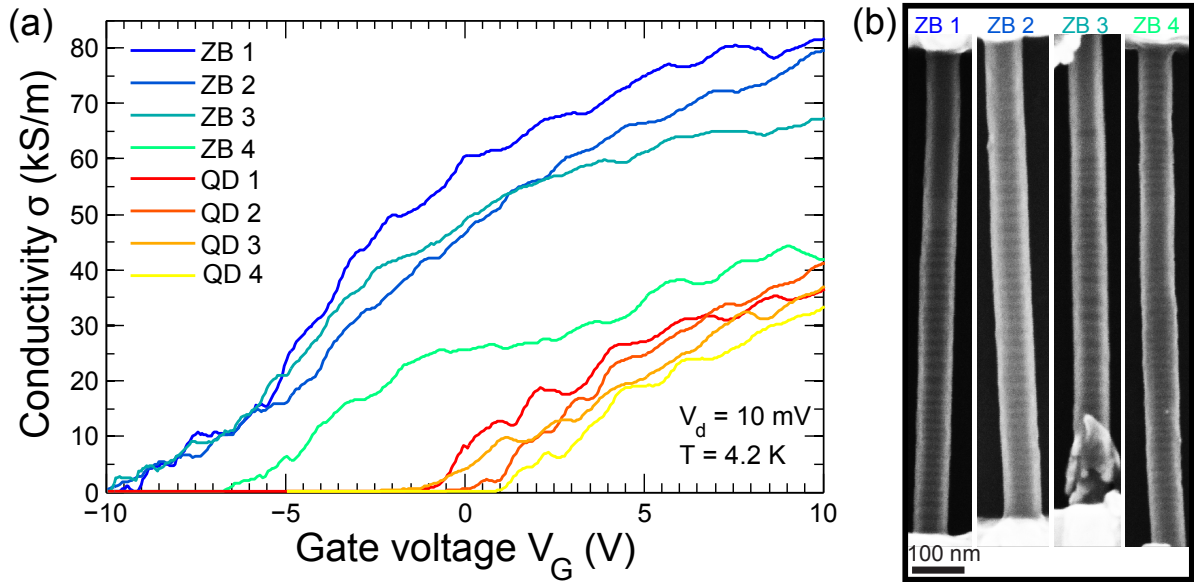


FIG. 1: (a) Conductivity as a function of gate voltage for four reference ZB segments (blue-green color scale) and for four QD devices (red-yellow color scale). (b) SEM images of the ZB reference devices optimized to see the twinned segments.

Figure 2 shows SEM images with different tilt angles of the sample holder for three different QD devices. At optimum tilt angle, the WZ segments can give rise to dark or bright contrast depending on device. In (a) both the WZ segments (red) and the twinned segments in ZB (arrow) appear when adjusting the tilt angle. In contrast, in (b) no twinned segments are visible at the optimal tilt angle (5°) to observe the WZ segments. The twinned segments instead appear at a different angle (-3°). In the case of (c) the WZ segments are visible at 6° and 12° , whereas twinned segments appear at 9° . Here it should be mentioned that the extracted dimensions are very sensitive to drift during imaging. In order to limit the error fast scan-speeds has been used when extraction dimensions. Figure 3(a) show the same SEM images as Fig. 4(c) in the text with an addition of an intensity profile (b) along the growth direction of the nanowire.

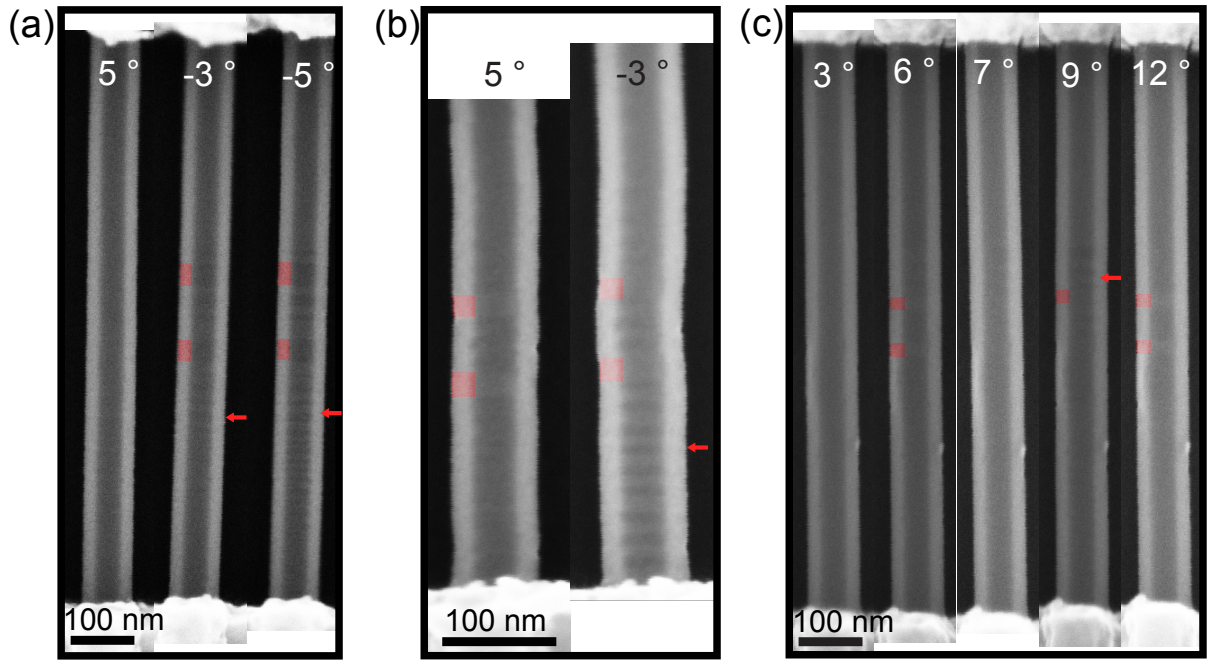


FIG. 2: (a) (c) SEM images of three different QD devices at different tilt angles of the SEM stage. When visible, the WZ segments are colored red, and tilt angles where twinned segments in ZB are visible are indicated by arrows.

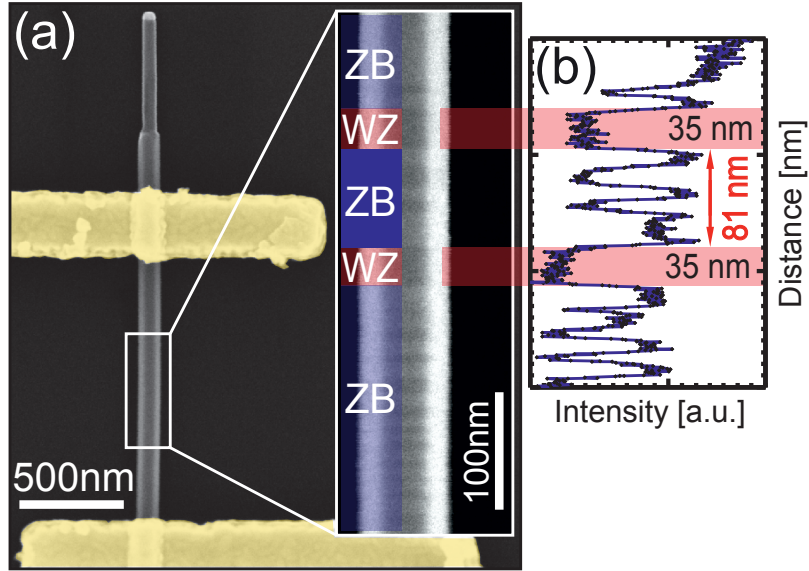


FIG. 3: (a) SEM images from Figure 4(c) in the main text with corresponding intensity profile (b).